Deciphering complex features in STM images of O adatoms on Ag(110)

Takat B. Rawal,[1] Marco Smerieri,[2] Jagriti Pal,[2,3,4] Sampyo Hong,[1,5] Matti Alatalo,[6] Letizia Savio,[2] Luca Vattuone,[2,3] Talat S. Rahman,[1,7] and Mario Rocca[2,3]

[1]*Department of Physics, University of Central Florida, Orlando, Florida 32816, USA*
[2]*IMEM-CNR, UOS Genova, Via Dodecaneso 33, 16146 Genova, Italy*
[3]*Dipartimento di Fisica, Università di Genova, Via Dodecaneso 33, Genova, Italy*
[4]*Fritz Haber Institute der Max Planck Gesellschaft, Faradayweg 4–6, Berlin 14195, Germany*
[5]*Division of Physical Sciences, Brewton-Parker College, Mount Vernon, Georgia 30445, USA*
[6]*Nano and Molecular Systems Research Unit, University of Oulu, P.O. Box 8000, FI-90400 Oulu, Finland*
[7]*Department of Applied Physics, Aalto University, FI-00076 Aalto, Finland*

(Received 10 November 2017; revised manuscript received 27 March 2018; published 2 July 2018)

Recently it was demonstrated that atomic oxygen can cause the extraction of substrate atoms off metal surfaces thus generating chemically different active sites. For Ag(110) this process occurs when O_2 is dosed at 175 K leading, at low coverage, to the formation of single Ag vacancies. Vacancy creation proceeds thereby via the formation of O-Ag-O complexes, which involve a local reconstruction of the surface and ignite the disruption of the Ag substrate. In this paper, we report on the details of such processes and on the isolated structures formed by the O adatoms in the limit of very low coverage. We employ scanning tunneling microscopy and density functional theory to unravel the complex structures of O/Ag(110) which are transiently present under specific reaction conditions. A variety of features such as isolated gray dots, sombreros, shallow gray and white structures oriented along [001] and [1$\bar{1}$0], gray stripes, and lozenges were identified and assigned to O adatoms in different configurations. The zigzag chains interact strongly with the STM tip and are easily disrupted, giving rise to highly mobile, sombrero-shaped, isolated O adatoms also far away from the scanned area, i.e., from the current injection spot. Around 200 K, not only Ag vacancies, which are mobile with anisotropic migration, can merge together into rather complex features, but also the mobile Ag atoms are trapped by O adatoms, thus facilitating the formation of an oxygen-decorated Ag chain along [001] which ultimately induces the well-known added-row reconstruction.

DOI: 10.1103/PhysRevB.98.035405

I. INTRODUCTION

Silver is a unique material, used for catalyzing industrially relevant reactions such as dehydrogenation of methanol [1], partial oxidation of ethylene [2–4], and oxidation of formaldehyde [5,6] and propylene [7,8]. The importance of silver in influencing these reactions has inspired researchers to put significant efforts in gaining insights into the chemical activity of surface structures of O/Ag systems. For example, the active O species responsible for ethylene oxide formation on Ag(111) [9,10] were recently identified, but the mitigating processes are still far from being fully understood [11,12]. One obstacle in the advancement of knowledge about the reactivity of the Ag catalyst in an oxidative environment is the complexity of the O-Ag system: the intricacy of the structures often involves the adsorption configurations of O species, inducing substrate reconstruction [13], oxygen migration to the Ag subsurface region [10,14], and formation of surface oxide phases [15].

Molecular oxygen adsorbs dissociatively on low Miller index Ag surfaces at crystal temperatures $T > 150$ K [16–19]. On the anisotropic Ag(110) face, in particular, substrate atom mobility sets in only at $T = 200$ K, leading to the formation of the well-known added-row reconstruction, consisting of -O-Ag-O-Ag- chains extending along the [001] direction [20,21] [i.e., across the atomic rows of the substrate; see surface geometry in Fig. 1(a)]. On the same surface, for $150\ \text{K} < T < 200\ \text{K}$, dissociative O_2 adsorption can lead to the formation of an O species with a higher chemical activity than both O_2 admolecules and O adatoms that are embedded in the added rows [22]. In the low-coverage limit, indeed, different isolated features corresponding to the different O species are revealed by scanning tunneling microscopy (STM) investigation [23–25]. We have recently demonstrated that shallow stripes extending in the [1$\bar{1}$0] direction (apparent depth from 0.1 Å to 0.5 Å)—referred to as gray stripes in the following and marked in Fig. 1(b)—are related to structures containing several O adatoms in a zigzag configuration. A deeper feature [0.7−1.0 Å deep, depending on measuring conditions; black dot (BD) in the following; marked in Fig. 1(b)] results from vacancies induced by dissociative adsorption of oxygen on Ag(110) [26]. These results clarified several unexplained observations such as the strong disordering of the surface upon O_2 dissociation [16] and the facile route by which oxygen migrates to subsurface sites even at low temperature [27]. Along the same lines, it is also likely that the strong reduction of the barrier for metalation of porphyrins on Cu surfaces in the presence of co-adsorbed oxygen [28,29] is associated with the grabbing of substrate atoms by atomic oxygen. As stressed in Ref. [26], these effects are not limited to Ag and Cu substrates, but are expected to occur for a wide category of metal substrates.

Nonetheless, a variety of O-related structures other than the two reported in Ref. [26] is observed on the O/Ag(110)

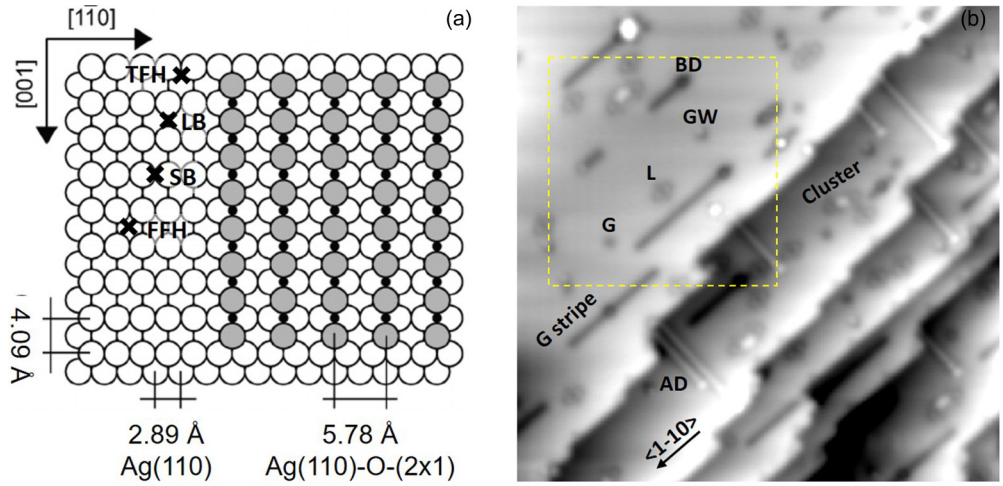

FIG. 1. (a) Geometry of the Ag(110) surface. The fourfold hollow (FFH), long bridge (LB), short bridge (SB), and threefold hollow (TFH) sites, relevant for the data presentation, are marked on the left part of the drawing. The structure of the Ag(110)-O-(2×1) added row reconstruction is shown on the right part. (b) STM image of the Ag(110) surface exposed to 19 L of O_2 at 175 K (image size: 25×25 nm^2, $V = 0.07$ V, $I = 1.3$ nA, virgin area). Black dot (BD) decorated by gray stripes, isolated gray dot (G_d), lozenge (L), added row (AD), gray and white dot oriented along [100] (GW), and isolated cluster structures are apparent on the terraces. The dashed box indicates the area subject to the manipulation experiment reported in Fig. 4. Added rows stretch along the [001] direction while G stripes have the axis aligned along [1$\bar{1}$0].

surface upon O_2 dissociation. Here, we provide a complete and detailed description of the structures formed on Ag(110) in the very low atomic oxygen coverage limit ($\Theta < 0.04$ ML) based on low-temperature high-resolution STM images and density functional theory (DFT) based simulations. The paper is organized as follows: we describe the experimental and computational details in Sec. I, we present our results from experiment and DFT simulation in Secs. III and IV, respectively, and we summarize our findings in Sec. V.

II. EXPERIMENTAL AND COMPUTATIONAL METHODS

The low-temperature STM (LT-STM; CreaTec) employed to perform the present experiments is hosted in an ultrahigh vacuum apparatus thoroughly described in Ref. [30]. O_2 dosing was performed by backfilling the chamber. The attained coverage was evaluated *a posteriori*, by statistical analysis of large STM overviews. The estimated value is compatible within the errors with the one expected, *a priori*, considering an O_2 sticking coefficient $S \sim 2\times10^{-3}$, according to previous literature [31,32].

The Ag(110) single crystal was prepared by repeated cycles of ion bombardment with 1.5 keV Ne^+ ions and annealing to 800 K for 5 minutes, until clean large terraces were observed by STM. STM images were recorded either at liquid nitrogen or at liquid helium temperature, using constant current mode and tunnelling current between 0.5 nA $< I <$ 2.0 nA. The bias voltage applied to the sample was varied between $-1.20\,\text{V} \leqslant V \leqslant 1.20\,\text{V}$. Scanning at $|V| = 0.56$ V resulted in surface disruption also far away from the scanned area as we will show later. Most of the images were therefore recorded for $V = \pm0.07$ V and ∼1 nA, which corresponds to a charge injection of some 6×10^8 electrons per surface unit cell. At such low voltage, local manipulation of the oxygen atoms could be achieved with a roughly 3 order of magnitude larger charge injection.

The STM tip is a Pt-Ir wire of 0.2 mm diameter, cut in air under strain. During the measurements, the tip apex is reshaped by controlled crashes into the Ag sample, so that tunneling occurs effectively through a silver tip. The piezo constants were calibrated on the basis of the Ag lattice parameter from atomically resolved images of the clean surface. The interplay of the various electronic effects can change the contrast of STM images as demonstrated, e.g., in Refs. [33,34]. Indeed we observed such effect occasionally but the modification was not stable enough to allow collecting images over large areas. The conclusions of the present investigation are, therefore, limited to the analysis of data recorded with a metallic tip. Analysis of the images was performed using both the acquisition software supplied by Createc and the WSxM software [35].

Density functional theory (DFT) calculations were performed using the Vienna *ab initio* Simulation Package (VASP) [36,37]. The exchange correlation of electrons was treated within the generalized gradient approximation with the PBE [38] functional. The projector augmented wave method [39] was adopted to account for the ion-electron interaction. Periodic (3×4), (4×4), and (6×8) supercells of Ag(110) were constructed using the calculated bulk lattice constant of 4.147 Å and setting the vacuum of 15 Å. The energy cutoff was set to 500 eV for the plane-wave expansion. All atoms were allowed to relax freely including the adsorbates until the total energy is converged to 10^{-5} eV, and the residual force on each atom is below 0.01 eV/Å. For the relaxation of the geometries of the (3×4), (4×4), and (6×8) unit cells, (7×7×1), (6×7×1), and (4×4×1) k-point meshes, and for the simulation of STM images, (21×21×1), (18×21×1), and (9×9×1) k-point meshes were employed, respectively.

The binding energy for oxygen per O atom adsorbed on Ag(110) is calculated using

$$E_b^{\text{O adatom}} = \frac{1}{n}[E_{[n\text{O/Ag(110)}]} - (nE_{\text{O}} + E_{\text{Ag(110)}})],$$

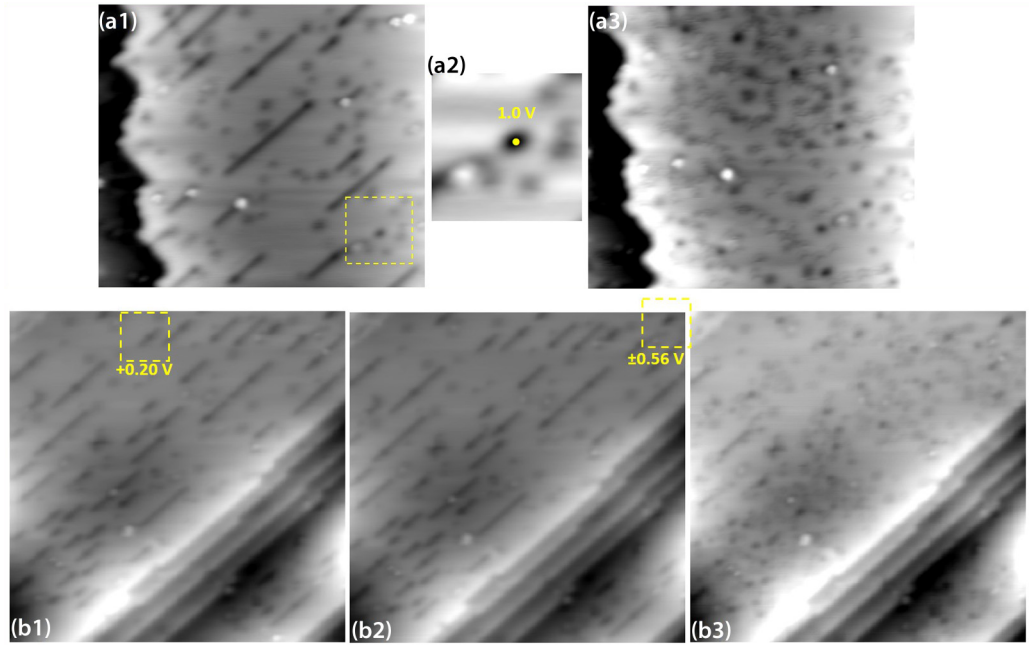

FIG. 2. Overviews showing the disruption of the surface upon interaction with the tip above a critical bias voltage. (a) STM images of the same region before (a1) and after (a3) applying a voltage ramp (from 0 to $V = 1.0$ V for a total of 600 ms with the tip retracted by 1 Å with respect to its position when acquiring images) on the vacancy site marked with the yellow dot in the enlarged panel (a2) [corresponding to the area in the dashed square in (a1)]. $V = 0.07$ V, $I = 1.3$ nA, image size: 34×30 nm^2 for (a1) and (a3), 7.0×7.0 nm^2 for (a2). The fuzzy appearance of the image in (a3) may be associated with the functionalization of the tip, most probably from the adsorption of an oxygen atom. Disorder over a wide area is however evident. (b) Sequence of STM images showing the consequences of scanning above a critical voltage on small areas (yellow dashed square, 5.0×5.0 nm^2): (b1) before scanning; (b2) after scanning the marked area in (b1) with a maximum voltage $V = 0.20$ V, 1.0 nA. No changes in the surface morphology are observed. (b3) After scanning the marked area in (b2) with a maximum voltage $V = \pm0.56$ V. The damage is now evident and extends over an area much larger than the scanned one.

where n represents the number of O adatoms per surface unit cell, and E_O, $E_{Ag}(110)$, and $E_O/Ag(110)$ represent the total energies of the isolated O atom, the pristine surface, and the adsorbate-substrate system, respectively. Based on this expression, the adsorbed oxygen that has a negative value of binding energy is stable. Note that this expression has a different sign convention from that found in an earlier study [40] for calculating the same quantity on Ag(111). Similarly to the procedure adopted in Ref. [40], spin-polarization corrections to the isolated, free atomic oxygen were included in total energy calculations.

The Tersoff and Hamann (TH) model [41] was applied to simulate STM images at low bias voltage, V. At higher V, the simulated STM images were approximated by the DFT-calculated isosurface (with isovalue of 10^{-4} $e/$Å^3) of the local density of states (DOS) integrated over the sample states from $-V$ (in eV) to the Fermi level.

III. RESULTS AND DISCUSSION

A. Experimental STM

Figure 1(b) shows an area of the Ag(110) surface after exposure to 19 L of O_2 at 175 K and cooling to 6 K. The atomic oxygen coverage estimated from STM images is ~0.02 ML [in monolayers of Ag(110); 1 ML corresponding to 8.4×10^{14} atoms/cm^2]. A variety of O-related features is evident on the surface: (i) 0.8 Å deep BD with 0.4 Å deep gray stripes [the latter sometimes appear as isolated gray dots (G_d)]; (ii) 0.2 Å deep lozenge-shaped structures (L); (iii) gray and white couples oriented along [001] (GW[001]); (iv) a few additional protruding objects (cluster). The initial formation of added -O-Ag-O-Ag- rows is evident at the lower side of steps. These added rows originate from Ag atoms released from the step edges and are imaged with atomic resolution. As demonstrated in our previous publication [26], G stripes correspond to zigzag rows of oxygen adatoms in threefold hollow sites while BD are single vacancies produced by adatom extraction. The other structures will be described in the following.

Before providing the details of the observed structures, it is necessary to point to some ambiguities, which have prevented a full understanding of the O/Ag(110) system so far. The STM investigation of the system is indeed extremely delicate since scanning above a critical bias voltage ($|V| \geqslant 0.7$ V) destroys the surface layer. This effect, first reported in Ref. [26], is particularly pernicious, since it is evident only in images recorded close to liquid helium temperature (6 K) and at low V. It was therefore not discerned in previous investigations [23,24]. In the following we will mainly concentrate on measurements recorded at ±0.07 and ±0.70 V sample bias.

Figure 2 shows STM images recorded after the same preparation as in Fig. 1 and evidencing the effect of tip-surface interaction. Panel (a1) shows a virgin area (i.e., not yet scanned by the STM tip) in which several different features, including BDs and gray stripes, are present. A voltage pulse with $V = 1.0$ V is eventually applied on the vacancy site marked by the

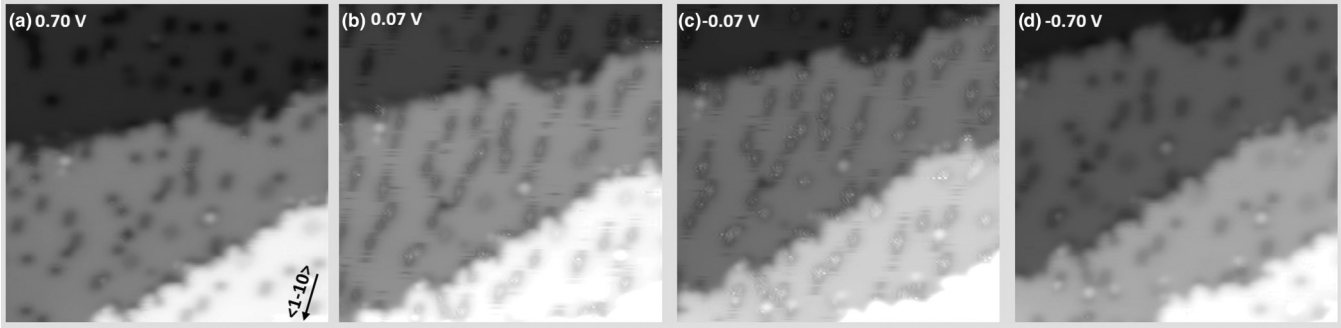

FIG. 3. Sequence of STM images of the Ag(110) surface exposed to 18 L of O_2 at 180 K recorded at different V ($I = 1.0$ nA, image size: 22.5×22.5 nm^2) and at $T = 77$ K. At low bias voltage [panels (b) and (c)] short stripes are present in the scanning direction (horizontal) due to the movement of weakly bonded oxygen adatoms under the tip while the image is recorded. Such effect is absent in the images collected at $V = \pm 0.7$ V [panels (a) and (d)] since the apparent depth of sombreros is then smaller (see Fig. 8 below).

yellow dot in the enlarged panel (a2) and the whole area is imaged again [panel (a3)]. It is evident that the stripes have now disappeared while the BDs are unaffected. The surface is now covered by sombrero-shaped objects (S) corresponding to single O adatoms. This assignment is demonstrated by our recent publication [26] and by a previous experiment by Hahn and Ho [42–44], who produced very similar features by disrupting chemisorbed O_2 admolecules by voltage pulses at 13 K. No sombreros are present on virgin areas, i.e., prior to the vertical manipulation process, implying that they are unstable as isolated features when dissociation occurs at 175 K.

The sequence of STM images reported in panels (b) shows the consequences of scanning above a critical voltage on a small area (marked by the yellow dashed squares). As evident, no changes in the surface morphology are induced upon interaction with the tip at $V = 0.20$ V [panel (b2)], while rastering the small region in the top-left corner with $V = \pm 0.56$ V causes a disordering of the adsorbed layer which extends over a much larger area [panel (b3)]. Sombreros are found up to 40 nm away from the scanned region, indicating that their formation is a surface-mediated phenomenon. A similar effect was reported by Hahn *et al.* [45], or tip current induced dissociation of O_2 chemisorbed on Ag(110) at 13 K, but it was unexpected in the present case since the initial state consists of already dissociated oxygen.

Figure 3 shows a similar experiment, in which subsequent STM images of the same surface area were recorded at different bias voltage and at liquid nitrogen temperature (77 K). While the position of O-related structures remains unchanged through the sequence, short stripes in the scanning direction are evident in the images at $V = \pm 0.07$ V. We interpret them as due to sombrero features rapidly moving below the tip, i.e., too mobile to be imaged at liquid N_2 temperature. Similar stripes were observed in Refs. [23,24] (in images recorded at 110 K) and assigned to O_2 admolecules. As it is improbable that admolecules survive annealing to 175 K, such possibility is excluded in our experiment, since oxygen exposure was performed directly at 175 K and the sample remained at that temperature for a prolonged time. In the same publications, sombrero-shaped objects were also observed but left unassigned. However, such features must be qualitatively different from the present ones, since they can be clearly imaged at $T = 110$ K with a typical bias voltage of 1 V.

To better characterize the behavior of the above described features we performed manipulation experiments reported in Fig. 4, starting from the surface area marked by the yellow box in Fig. 1. Column (a) refers to manipulation over a BD and the associated gray stripe. Upon vertical manipulation on a BD [yellow mark on panel (a1)], i.e., by applying a voltage pulse with $V = +0.07$ V and 1 nA for 200 ms (corresponding to roughly three orders of magnitude larger electron dose per unit cell than when collecting an image by rastering), the gray tail is shortened by two lattice spacings [26] and two sombreros, initially absent from the surface, are generated [panel (a2)]. The gray tail corresponds therefore to oxygen atoms. The second pulse, applied directly on the far left end of the gray tail, causes again the generation of two sombreros and the corresponding shortening of the tail by two lattice spacings [panel (a3)]. The procedure is repeated until only the BD remains. A secondary effect of the voltage pulses is to swap the white and the gray part of the GW structure marked by the arrow in panel (a3).

The manipulation sequence of column (b) is performed on the same area to better characterize the behavior of sombreros. It shows that two sombreros can approach each other in a controlled way and merge to form a GW feature oriented along the $[1\bar{1}0]$ direction [see white arrow in panels (b2)–(b4)], which is reproduced by DFT as an O-Ag-O complex embedded in the Ag surface (see Fig. 10). While the protrusion remains fixed, the position of the depression can be swapped by further manipulation [compare panels (b3) and (b4)], obtaining an object with a specular profile (line scans GW1 and GW2). The GW feature generated by manipulation can be separated into its original components, as demonstrated by panels (c1) and (c2). In addition, the same images show that two sombreros can merge forming a GW oriented along the [001] direction [white arrow in panels (c2) and (c3)]. Finally, the isolated G_d in the bottom-left quarter of the image presents an apparent depth comparable to the GW structures but the additional side protrusion is missing [see line scans at the bottom of column (b)]. Therefore, it must correspond to a different configuration of oxygen adatoms.

In order to determine the relative positions of the observed features with respect to the underlying Ag(110) substrate, we exploited images such as those of Fig. 5, in which the O-related structures coexist with isolated added rows [see scheme in Fig. 1(a)]. The latter are imaged with atomic resolution and

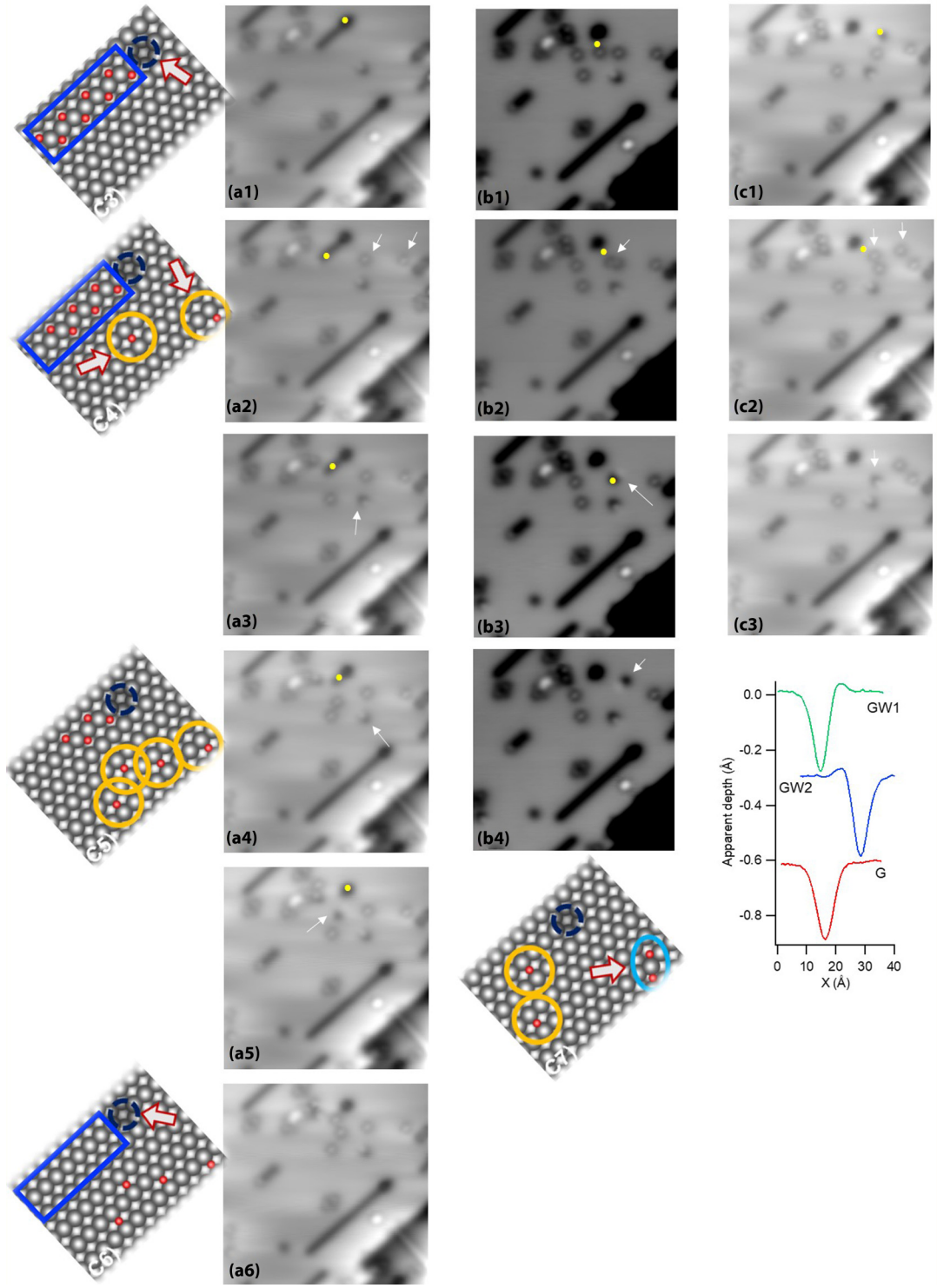

FIG. 4. STM images showing three manipulation sequences performed on different objects present in the same area. In sequence (a) sombreros are generated from the gray tail of a black dot by voltage pulses. Two new sombreros form for each pulse. In sequence (b) sombreros merge into a GW $[1\bar{1}0]$ structure. In sequence (c) such structure is broken again into two sombreros (for all images, size: $12.1 \times 12.1\,\mathrm{nm}^2$, $V = 0.07\,\mathrm{V}$, $I = 1.3\,\mathrm{nA}$; vertical manipulation parameters: 0.07 V, 1 nA, 200 ms applied to the positions marked by yellow dots). Schematic representations for the main processes are given, too. Left: The gray tail (-O-Ag-O-Ag-O- zigzag chain) is shown by a rectangular box. The shortening of the chain leads to two sombreros (isolated O adatoms at LB site), shown by circles. The continuous process shortening the tail gives rise to a black dot (isolated Ag vacancy), shown by dotted small circle. Bottom of column (b): Merging two sombreros into an O-Ag-O complex, shown by an oval. Bottom of column (c): Breaking of a pair of O adatoms (involved in the complex) into the original sombreros. Bottom of the column: Apparent depth profiles cut in the $[1\bar{1}0]$ direction across the manipulated GW structure of panels (b3) and (b4) and across the pristine gray dot located at the bottom left of the images. A more detailed description of the described events is reported in the Supplemental Material [46].

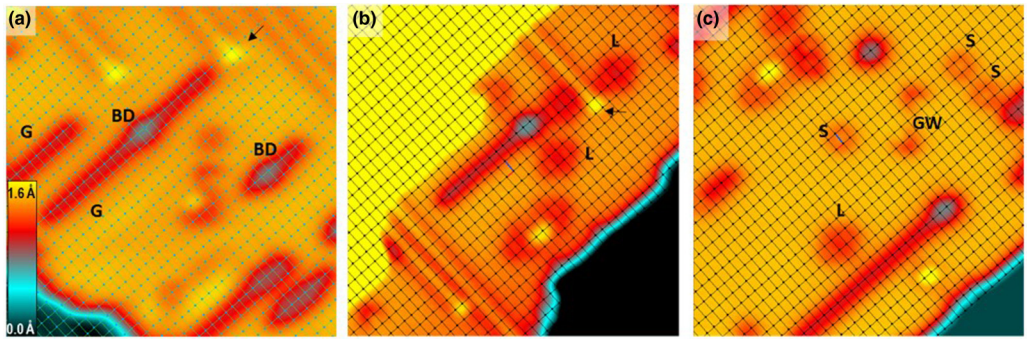

FIG. 5. STM images recorded after exposing the surface to 19 L O_2 by backfilling at 175 K. BD and G structures coexist with the added O-Ag rows extending along the [001] direction. The yellow spots (black arrow) correspond to terminal Ag atoms of added rows, which are known to be at hollow sites. Taking these features as a reference, a grid corresponding to the Ag lattice is superimposed on the image. Both BD and G structures are located on top of the Ag rows [panel (a)]. The same procedure allows us to locate the center of the lozenges (L) at hollow sites [panel (b)] and sombreros (S) at long bridge sites [panel (c)]. For all images, size: 100×100 Å^2, $V = 31$ mV in (a) and 0.07 V in (b) and (c). Bottom-left inset: Color scale for the apparent height. Taken from the Supplemental Material of Ref. [26].

always terminate with a brighter spot, which corresponds to an Ag atom [47]. Since it is well established that the Ag atoms in the added rows sit in the hollow sites (H) of the unreconstructed Ag(110) plane, we can use this structure as a reference to draw a grid corresponding to the lattice of the unreconstructed Ag(110) plane underneath (Ag atoms are located in the intersections of the grid). From this construction, we can determine that BDs and gray stripes sit on top of the atomic rows of the Ag substrate [Figs. 5(a) and 5(b)]. Lozenges, on the contrary, have their long axis in the valley and their center in an H site, while sombreros are adsorbed at LB sites. The position of isolated gray dots is more difficult to determine. They seem to sit in the on-top position, but more statistics on high-resolution images would be needed for a careful assignment. Similarly, we are not able at the moment to identify the position of the GW[001] features with accuracy.

We observe that the two BDs in Fig. 5(a) appear slightly elongated along [1$\bar{1}$0] and that their center lies at a short bridge (SB) site. On the contrary, the BD in panel (c), obtained by "cleaning" off its gray tails by voltage pulses as described in Fig. 4(a), appears round and its center coincides with an Ag lattice site. We conclude that BDs may correspond either to pairs of vacancies (elongated features) or to single vacancies (round BD). Thus, merging of vacancies takes place already at 175 K, implying that Ag atoms have some mobility already at this temperature. Short-range Ag atom mobility is not surprising and is witnessed also by the appearance of some short added rows at the lower side of step edges.

Vacancies are efficient pinning centers for the gray stripes. We remark that also residual O_2 admolecules are imaged as 0.4 Å deep indentations [42–44], and that they would also release two oxygen atoms upon disruption. However, in our experimental conditions, the assignment of gray features (pristine dots and stripes) to atomic oxygen is straightforward since the presence of admolecules is ruled out by the dosing temperature, as discussed above.

Lozenges (L) appear as slight indentations with two lobes and are observed at any bias voltage in the investigated range (see Fig. 6). These features, more abundant in stepped areas, first appear at $T > 170$ K and can be associated with some reconstructive geometry of O and Ag atoms [23], as will be shown in Fig. 13.

Figure 7 shows two additional features seldom observed upon the same preparation. As evident in the enlargement of panel (b) and from the line profiles of panel (c), the former (1) appears as two half-lozenges at the opposite side of a protrusion, probably an Ag adatom trapped in between them. In case (2), the same structure is sided by gray dots. These structures correspond most probably to the "clusters" reported in Ref. [24]. The latter feature (3) is a rectangular-shaped

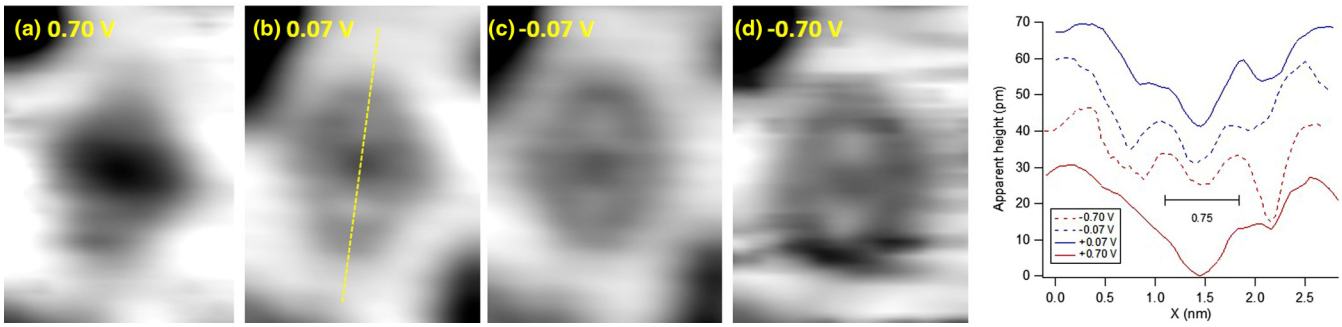

FIG. 6. STM images showing lozenges recorded at different tip bias ($I = 1.0$ nA, $T = 6$ K, image size $= 2.2\times3.0$ nm^2) and corresponding line profiles cut along the [1$\bar{1}$0] direction, i.e., along the major axis of the lozenge. The distance between the center of the lobes in this direction is 7.5 Å.

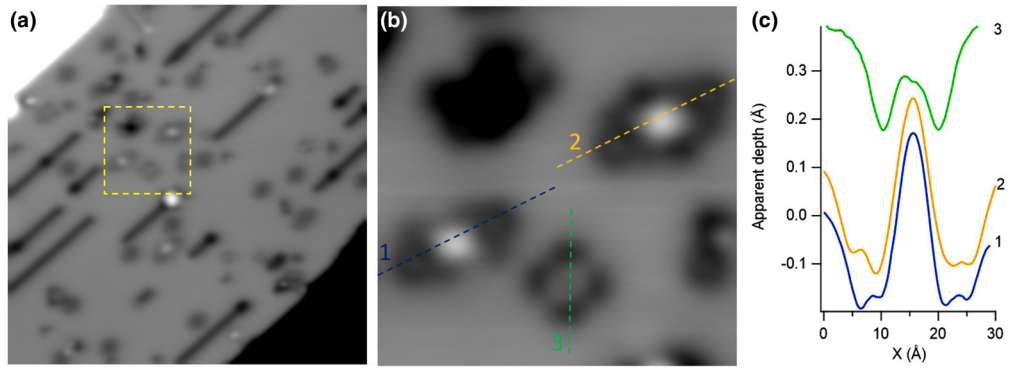

FIG. 7. (a) STM overview ($25\times25\,\mathrm{nm}^2$, 70 mV) of the Ag(110) surface after exposure to 19 L of O_2 at 175 K. (b) Enlargement of the area marked by the dashed yellow square in (a) ($6.0\times6.0\,\mathrm{nm}^2$, 1.3 nA, 70 mV). Images are recorded at 6 K. The additional cluster features discussed in the text are evident. (c) Height profiles cut across the different O-related structures following the path marked by the corresponding dashed lines in (b).

object reminiscent of four close-by gray dots. However, it was observed also in between a (6×1) added row reconstructed surface produced by O_2 exposure at room temperature and can be imaged at $V \geqslant 1.0$ V [47]. In view of this particular behavior, we believe that it is probably an O-related feature but with a different nature with respect to gray dots.

B. DFT and kMC simulations

In order to unravel the objects observed experimentally, as in our previous joint publication [48], we have carried out density functional theory based calculations to obtain the following for various configurations of the O/Ag(110) system: relaxed (ionically) geometry, energetics and activation energy barriers of several relevant phenomena (adsorption, vacancy formation, diffusion), and simulated STM images. Note that these detailed results have not been reported in our earlier publication [48]. We discuss first the simulated STM images.

1. Simulated STM images

a. Isolated O adatoms. Figure 8 shows the optimized geometries, the simulated STM images, and the corresponding line profiles of O adatoms at fourfold hollow [FFH, panel (a1)], long-bridge [LB, panel (a2)], and threefold hollow [TFH, panel (a3)] sites. The details of the geometrical parameters and adsorption energy of the O adatoms can be found in Ref. [48]. The simulated STM images at $V = 70$ mV [column (b)] and 700 mV [column (c)] are compared with available experimental data [column (d)] as follows:

(i) An O adatom at the FFH site (upper panel, Fig. 8) appears as a depression in the STM image with 0.4 Å depth in the profile simulated at $V = 70$ mV and as a relatively shallow contrast at 700 mV, thus showing a good agreement with the line profile of the gray dots measured at $V = 70$ mV (see the measured line profile in Fig. 4). At $V = 700$ mV, however, as mentioned above this species is not stable under the STM tip; thus no experimental data are available to compare with the calculated one.

(ii) O at the LB site appears as a sombrero-like object in the simulated STM image at 70 mV [see Fig. 8(b2)]. It is characterized by two equivalent 0.25 Å deep indentations on both sides of the O adatom as seen in the corresponding depth profile. Therefore, the experimentally observed S feature in Fig. 5(c) can be safely assigned to such O/Ag configuration. At $V = 700$ mV, however, the calculated STM image shows a smaller contrast with shallow depth in the calculated profile [see Figs. 8(c2), 8(d2)]. The comparison of the STM simulation for $V = 700$ mV with experiment is also not possible since the S structures cannot be imaged at the corresponding measuring conditions.

(iii) The STM image of the O adatom at the TFH site simulated at 70 mV has a shallow gray and white feature [Fig. 8(b3)] characterized with a 0.3 Å indentation in the calculated profile. This feature becomes more evident at $V = 700$ mV [Fig. 8(c3)]. The bright lobe, however relatively smaller than the protruding features of surrounding Ag atoms, corresponds to the exact location of the O adatom while the gray shadow is on the other side of the atomic row. Though this feature resembles the GW[001] one observed experimentally, we believe that the similarity is fortuitous since experimentally the GW is produced by merging two sombreros together [see Fig. 4(c)], while only one O adatom is involved in the simulated structure.

At variance with our conclusions, Hahn and Ho [43] indicated that S features were related to O adatoms at hollow and short bridge (SB) sites, which were generated by dissociating chemisorbed O_2 with voltage pulses at 13 K. Oxygen at the SB site was said to generate a two-lobe rather than a circular feature, and to be able to jump from one SB to another on a neighboring row without falling into the much deeper potential wells in between. Our STM simulations indicate, however, that O adatoms at SB sites should appear as protruding features in the STM image with ∼1 Å of height from the surface (not shown here), but also that this site is unstable with respect to lateral displacements [48]. The results of Ref. [43] are also at variance with our experimental findings, which show that S features in STM images relate only to the O adatoms at LB sites. We cannot exclude, however, that O may end up at metastable sites when the adatoms are generated at 13 K from O_2 admolecules.

b. Gray stripes, GW oriented along $[1\bar{1}0]$*, and the observed cluster.* Figure 9(a) shows the optimized structure of O adatoms arranged at TFH sites in an -O-Ag-O-Ag- zigzag chain. The Ag atoms in contact with O adatoms are vertically displaced

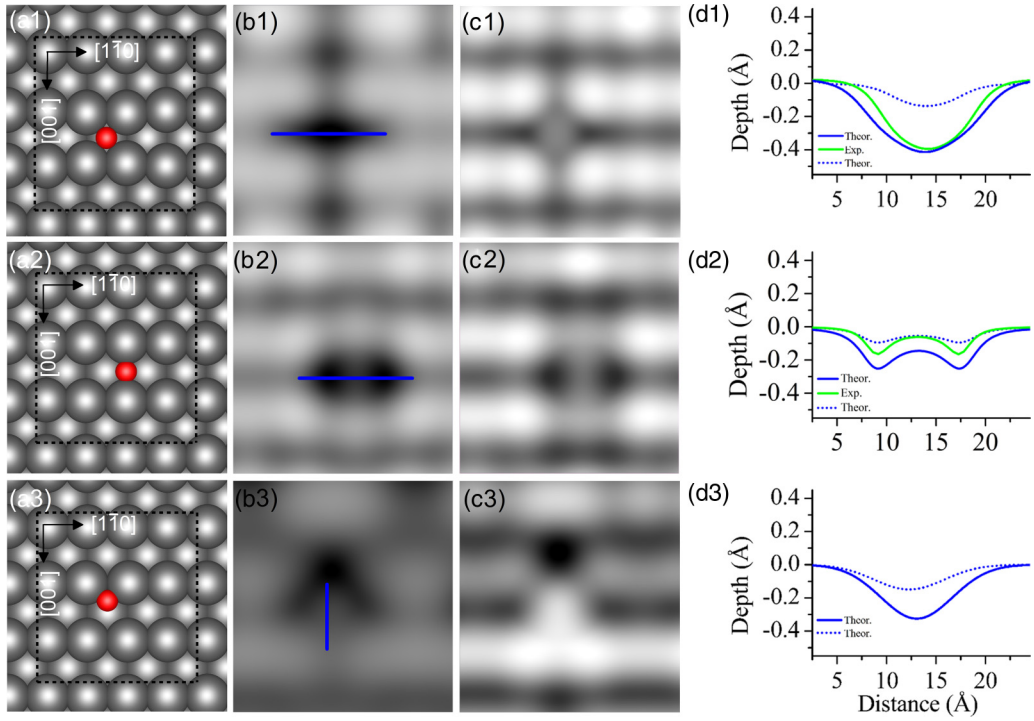

FIG. 8. (a1)–(a3) DFT-optimized geometries of O adatoms at (a1) FFH, (a2) LB, and (a3) TFH sites. (b1)–(b3) and (c1)–(c3): Corresponding simulated STM images at (b1)–(b3) $V = 70$ mV and (c1)–(c2) $V = 700$ mV, (c3) $V = 700$ mV. (d1)–(d3) Corresponding line profiles for $V = 70$ mV (blue solid line), $V = 700$ mV for (d1) and (d2) and 700 mV for (d3) (dashed line) collected along [1$\bar{1}$0] for (d1) and (d2) and along [001] for (d3). The experimental data recorded at 70 mV are reported for comparison (green line) when available.

by 0.55 Å with respect to their initial position. Such a local disorder in geometrical structure could be the consequence of the direct electrostatic interaction between Ag and O adatoms (involved in the chain). The local electronic structure varies upon the arrangement of O adatoms on the surface, thus yielding different STM features. Although the simulated STM image at 70 mV [Fig. 9(b)] corresponds to an internal structure corresponding to O adatoms at TFH sites, empty TFH sites, and Ag atoms in the proximity of O adatoms, on average the whole zigzag structure appears as a depression of 0.4 Å in the depth profile [Fig. 9(d)], with respect to the surrounding Ag atoms. Hence it can be associated with the gray stripe (G) features observed experimentally [see Fig. 5(a)]. At $V = 700$ mV, the image contrast changes and O adatoms become slightly protruding but less than the neighboring Ag atoms (consistent with the calculated density of states for O and Ag atoms, as shall be described later), while the zigzag shape of the structure is still preserved [Fig. 9(c)]. The STM simulation for 700 mV cannot be compared with experiment since the gray stripes are disrupted at this bias.

Figure 10 shows the optimized geometries, the simulated STM images at $V = 70$ mV and at 700 mV, and the corresponding line profiles of two different O-Ag-O complexes: embedded [panels (a1)–(d1)] and free [panels (a2)–(d2)]. First, the one reported in Fig. 10(a1) ("embedded" in the following) involves one Ag atom of the surface, which is lifted by 0.56 Å from the surface plane, and two oxygen atoms in nonequivalent sites. The simulated STM images [Figs. 10(b1)–10(c1)] and the line profiles [Fig. 10(d1)] compare nicely with the GW[1$\bar{1}$0] features observed experimentally [see Fig. 4(b4) and the

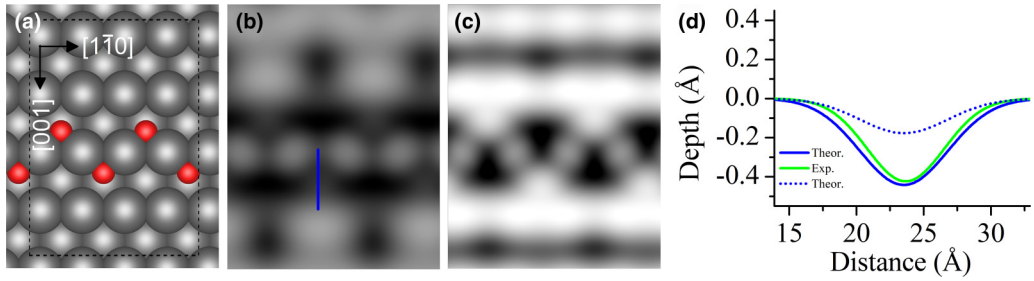

FIG. 9. (a) Optimized geometry of O adatoms at TFH sites and organized in an -O-Ag-O-Ag- zigzag chain. (b) and (c) Simulated STM images at $V = 70$ mV and $V = 700$ mV, respectively. (d) Line profiles cut along the [001] direction [blue path in panel (b)]. The blue solid and dashed traces derive from the simulated images at $V = 70$ mV and $V = 700$ mV, respectively. The experimental curve recorded at 70 mV is plotted in green. No experimental trace is available for $V = 700$ mV since at this bias voltage the gray stripes are disrupted.

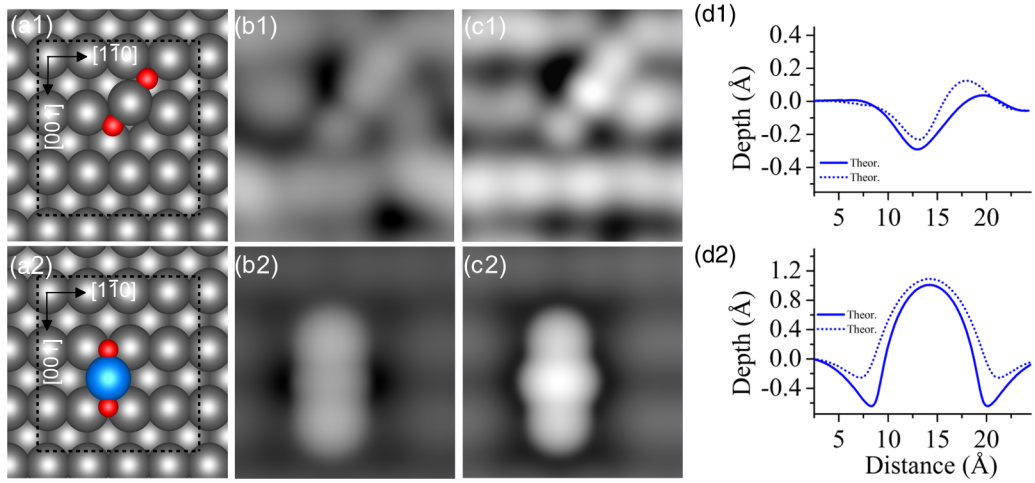

FIG. 10. (a1) Optimized geometry of an O-Ag-O complex forming upon O_2 dissociation on Ag(110). (b1) and (c1) Simulated STM images at $V = 70$ mV and $V = 700$ mV, respectively. (d1) Line profiles cut through the Ag adatom along [1$\bar{1}$0] for $V = 70$ mV (solid trace) and 700 mV (dashed trace). (a2)–(d2) Same as (a1)–(d1) for the free O-Ag-O complex.

measured line profile]. Second, the free O-Ag-O complex, which can be formed upon the detachment of an embedded O-Ag-O complex and the extraction of an Ag atom, consists of an Ag adatom with two side oxygen atoms oriented along the [001] direction ("free" complex in the following). Note that the detachment process is slightly endothermic and can therefore occur spontaneously only thanks to the entropic contribution to the free energy. Based on our simulation, the detached O-Ag-O complex appears as a dumbbell in the simulated STM image at 70 mV [Fig. 10(b2)] and is characterized by 0.3 Å depth in the calculated line profile. On the other hand, the simulated image at 700 mV appears as a relatively intense protruding feature with slight change in shape and characterized by ∼1 Å apparent height in the calculated profile [Figs. 10(c2)–10(d2)]. If there are not enough O adatoms for the formation of extended added rows, these O-Ag-O complexes may merge with semi-lozenges or lozenges (as shall be described later).

Next, we simulated the STM image for the structure involving an oxygen atom buried in the octahedral interstitial immediately below an Ag atom [shown by the pink ball, Fig. 11(a)]. Our simulation indicates that such O atom together with the vertically displaced Ag atom relates to the enhanced protruding features in simulated STM image at both $V = 70$ mV and 700 mV [see Figs. 11(b), 11(c)], characterized by 2.4 Å and 1.8 Å heights in the line profile [Fig. 11(d)]. This feature could partly contribute to the cluster structures observed in the experiment [Fig. 7(b)].

c. Lozenges. One of the most common features at low O coverage is the lozenge [experimental data reported in Figs. 5(b) and 6]. The O adatoms placed in the valley at 2.5 lattice spacing from one another eventually move to the FFH sites at which the structure is relaxed. The energy minimization obtained by allowing all degrees of freedom to relax thus fully reproduces the L structure. We then relax the configuration in which O adatoms are slightly off the FFH sites, by applying a constraint for O adatoms along one axis (only two degrees of freedom are allowed for relaxation). The model for lozenges is shown in Fig. 12(a). The STM simulation for such configuration produces a shallow indentation with two lobes sitting in the valleys, about 0.4 Å off FFH sites. The simulated image at 700 mV [Fig. 12(c)] has wider indentation as compared to that obtained with 70 mV. This difference could be attributed to the local electronic effects: more electrons of Ag may participate in tunneling current for 700 mV than for 70 mV bias. The simulated STM images both at $V = 70$ mV and 700 mV agree with the experiment. The shallow indentation in the calculated STM image is characterized by ∼0.25 Å. The calculated depth profiles nicely agree with the experiment [see Fig. 12(d)]. These results show that lozenges consist of two O adatoms which can be stabilized by some local distortion of the substrate. Moreover, we note that if not enough O adatoms

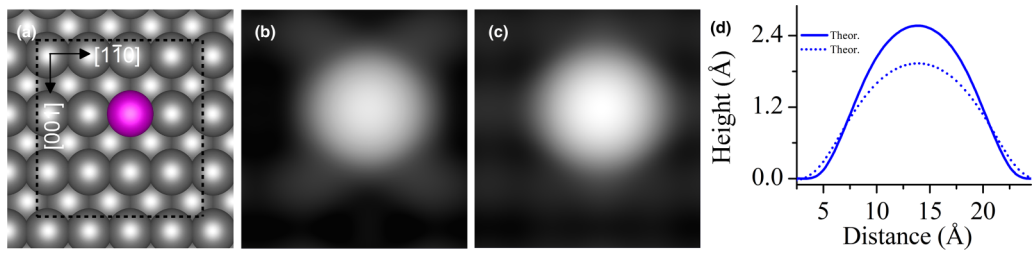

FIG. 11. (a) Optimized geometry of O residing at the octahedral subsurface site. The Ag atom (pink ball) is located just on top of a subsurface O atom. (b) and (c) Simulated STM images at $V = 70$ mV and $V = 700$ mV, respectively. (d) Line profiles (solid trace for 70 mV; dashed trace for $V = 700$ mV).

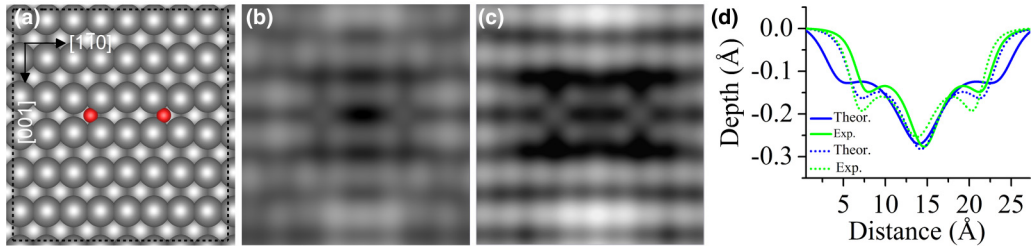

FIG. 12. (a) Optimized geometry of a configuration with two O adatoms positioned in the troughs of the Ag rows, slightly off the FFH sites, forming the lozenge (L) shaped objects. (b) and (c) Simulated STM images at $V = 70$ mV and $V = 700$ mV, respectively. (d) Line profiles in the valley along [1$\bar{1}$0] (solid trace for 70 mV; dashed trace for $V = 700$ mV).

are available on the surface for the formation of extended -O-Ag-O- added rows, "free" O-Ag-O complexes may merge into lozenges or semi-lozenges. Indeed, the compatible half-lozenge features were occasionally observed experimentally (see, e.g., Fig. 7).

2. Electron density of states

According to Lang's theory [49–51], the local density of states near the Fermi energy governs the contrast in the images of the individual adsorbates in STM. Oxygen will appear as a protrusion if it causes an increase in the local density of states compared to the silver substrate whereas it will be imaged as a depression if the local density of states is depleted with respect to the neighboring atoms on the surface.

The computed projected density of states (DOS) of the O adatoms at FFH and TFH sites, and of the Ag atoms (topmost layer) of the bare surface, is shown in Fig. 13. Here, the DOS of O adatoms is deduced from the contributions from 2s and 2p orbitals, whereas that of Ag atoms of the bare surface is only plotted for s orbitals since Ag s orbitals are spread evenly around the Fermi level (E_F) and thus can participate in the tunneling current. As shown in Fig. 13, the Ag 5s states are dominant over the O 2p states above the Fermi level, while the O p states are dominant over the Ag states at -0.7 eV (in reference to E_F). Since the DOS is smaller for O adatoms than for Ag atoms on the surface at 70 mV and larger at 700 mV sample bias, O adatoms will normally be imaged as depressions at low voltages and as protrusions at high voltages. Therefore, at very small bias voltage ($V < 0.1$) O adatoms should always appear as depressions in the STM images.

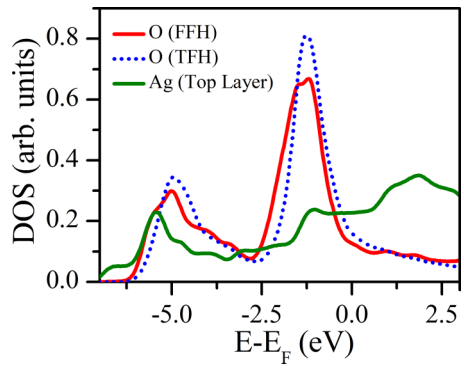

FIG. 13. Electron density of states projected on the 2s and 2p orbitals of an isolated O adatom at FFH site (red solid trace) and of an O adatom at TFH site embedded in the -O-Ag-O-Ag-O- zigzag chain (blue dotted trace) formed on Ag(110), and the 5s orbital of Ag atoms on the topmost layer (green trace) of the bare Ag(110). The energy is expressed relative to the Fermi energy (0 eV as reference level).

3. Oxygen adsorption, vacancy formation, and diffusion

a. Adsorption of O adatoms. The binding energies of O atoms in different configurations are summarized in Table I. Our calculations show that all considered isolated O adatom configurations are equally probable to appear on the surface since they have nearly the same binding energy to their respective sites and their wells are separated by 30–70 meV energy barriers [48]. Thus, it is not surprising that isolated O adatoms can be mobile on Ag(110). In addition, we find that O adatoms embedded in the O-Ag-O complex, the detached O-Ag-O complex, and the zigzag chain are slightly stronger in binding than isolated ones, having binding energies per O atom of -3.98 eV, -4.12 eV, and -3.99 eV, respectively. The binding energy of an isolated O adatom adsorbed at the slightly preferred FFH site is -3.88 eV, followed by an O adatom in TFH, and O in LB. On the other hand, the two O adatoms, adsorbed at slightly shifted FFH sites (responsible for the Lozenge feature, as discussed in Sec. III B 1 c), gain energy when they are in a pair (see Table I). This indicates that the geometric structures for O adatoms in a pair with binding energy per O atom of -3.97 eV are slightly preferred over those

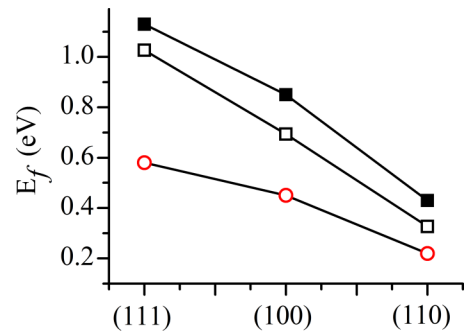

FIG. 14. Calculated vacancy formation energy per surface unit cell on the (111), (100), and (110) surfaces of Ag. DFT results are shown by solid squares, effective medium theory results [52] by empty squares, and results from the inserted-atom method [53] by empty circles.

TABLE I. Calculated binding energy and structural parameter for O adatoms adsorbed at different adsorption sites of Ag(110) with their STM features (compatible with the experiment described in Sec. III B 1) corresponding to different structures. $E_b^{\text{O adatom}}$ represents the binding energy per O atom, and $d_{(\text{O}-\text{Ag})}$ represents the shortest distance between the O adatom and first-nearest-neighboring Ag atom.

Structures	Adsorption sites	STM features	Supercell	$E_b^{\text{O adatom}}$ (eV)	$d_{(\text{O}-\text{Ag})}$ (Å)
Isolated O	FFH	Gray dot	(3×4)	−3.88	2.39
Isolated O	LB	Sombrero	(3×4)	−3.85	2.31
Isolated O	TFH	GW	(3×4)	−3.87	2.15
Isolated subsurface O	Subsurface octahedral	Whitish dot	(3×4)	−2.53	2.10
O-Ag-O complex	TFH	GW [1$\bar{1}$0]	(3×4)	−3.98	2.05
Detached O-Ag-O complex	SB (O also coordinated with Ag adatom in FFH)	Dumbbell	(3×4)	−4.12	2.03
Zigzag chain (-O-Ag-O-Ag-)	TFH	Gray stripes	(4×4)	−3.99	2.06
Isolated O pair	Shifted FFH	Lozenge	(6×8)	−3.97	2.25

structures in which the adatoms are isolated. Very distinct from isolated O adatoms and those in a pair, we find that an O in an octahedral subsurface site is energetically less favorable by 1.35 eV, 1.34 eV, and 1.32 eV than O adatoms in FFH, TFH, and LB, respectively. Thus, the various arrangements of O atoms result in different geometrical structures of O/Ag(110), suggesting different electronic and chemical properties.

b. Vacancy formation. We now turn to discuss the energetics of Ag vacancy formation on Ag(110). Figure 14 summarizes the vacancy formation energies on pristine low Miller index Ag surfaces, as calculated using three different theoretical methods: DFT (present study), the effective medium theory (reported in Ref. [45]), and the inserted-atom method (reported in Ref. [47]). The trend in the energetics for Ag vacancy formation on low Miller index surfaces is the same for all of the three methods considered. Strikingly, vacancy formation is found to be much easier on Ag(110) than on Ag(100) and Ag(111) owing to the fact that fewer Ag bonds need to be broken for this surface. We find that the process is, however, always endothermic. Note that the process will not take place on Ag(110) until $T \geqslant 175$ K owing to the activation energy for the process as shall be discussed later. At finite temperature, the quantity which must be minimized is the free energy $F = E - T\Delta S$. The endothermicity of the process can thus be easily overcome by the entropic term. For Ag(110), the vacancy formation already occurs at a relatively low temperature.

Creation of Ag vacancies is favored at higher oxygen coverage on Ag(110). Figure 15 depicts the calculated energetics of vacancy formation (i.e., Ag atom extraction) on Ag(110). It indicates that at low temperatures Ag atom extraction is not favorable unless O adatoms are present. As shown in Fig. 15(a), the forward process of Ag atom extraction needs to overcome a barrier of 0.69 eV, which is higher than the barrier of 0.27 eV for the backward process of filling the vacancy, and is also higher than the one for vacancy migration along [1$\bar{1}$0] of 0.47 eV. In contrast, when O adatoms are present on the surface they facilitate the extraction of Ag atom from the surface. Specifically, "O-atom-assisted concerted motion" reduces the barrier for vacancy formation to 0.52 eV for an oxygen coverage of 0.16 ML [two O adatoms per (3×4) surface unit cell], and further to 0.46 eV at 0.25 ML [three O adatoms per (3×4) surface unit cell], while the barrier for vacancy filling increases significantly [Figs. 15(b), 15(c)]. Therefore the presence of O adatoms on Ag(110) hinders the vacancy destruction process (see Ref. [26]).

c. Diffusion of Ag vacancies. On Ag(110), vacancies can diffuse and aggregate into more complicated features. The barrier for diffusion of vacancies is highly anisotropic: along [001] it is 0.80 eV whereas it is 0.47 eV along [1$\bar{1}$0]. The minimum energy diffusion pathways along both directions are shown in Fig. 16. These energetics suggest that at the temperatures in our experiments vacancy migration only along [1$\bar{1}$0] is active and leads to the formation of multiple vacancies when their concentration is sufficiently high. Vacancies can then merge forming the body of the "butterfly" structure which was previously described in Ref. [26].

4. Kinetics of vacancy formation

In order to gain insights into the kinetics of Ag vacancy formation, we performed kinetic Monte Carlo (kMC) simulations, the results of which are summarized in Fig. 17. For completeness, we also depict the number of events for O_2

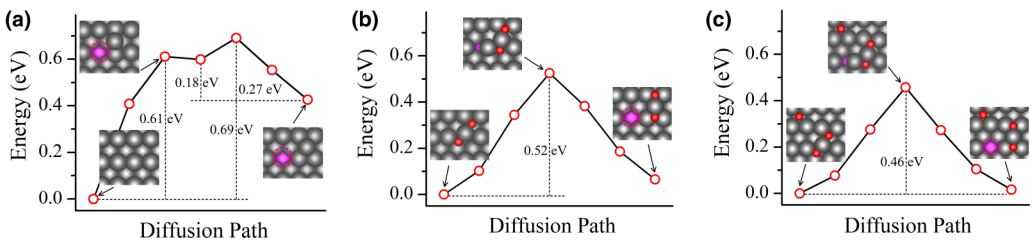

FIG. 15. Energetics of atom extraction from the Ag(110) surface: (a) in the absence of O atoms, (b) in the presence of 0.16 ML of O adatoms, (c) in the presence of 0.25 ML of O adatoms. Also shown are the activation energy barriers. The gray, pink, and red balls represent the Ag atoms of the top layer, the Ag atom of the third layer, and the O adatoms, respectively.

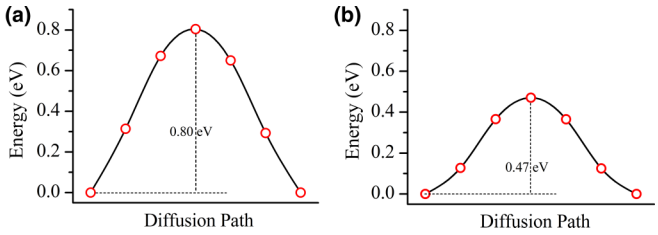

FIG. 16. Activation energy barriers for the diffusion of Ag vacancy on Ag(110) along (a) [001] and (b) [1$\bar{1}$0].

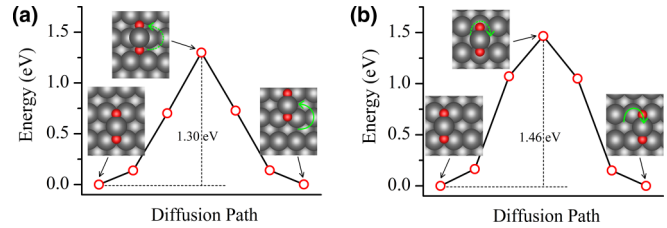

FIG. 18. Activation energy barriers of the detached O-Ag-O complex diffusion on Ag(110) along (a) [001] and (b) [1$\bar{1}$0] directions.

dissociation, which is a prerequisite for the vacancy formation process. As evident from the dotted blue curve, the maximum of O_2 dissociation events occurs at 157 K (for which the activation energy barrier is 0.42 eV [48]). Therefore, one could expect that, at $T \geqslant 157$ K, surface Ag atoms feel strong attractive interaction with the dissociated oxygen, which may enable the formation of "embedded" O-Ag-O complexes [note that the formation of the O-Ag-O complex is a spontaneous process on Ag(110)], and thus initiate the process of Ag vacancy formation. On the other hand, the solid red curve shows that the maximum of Ag-vacancy-formation events occurs at 190 K in the presence of 0.16 ML of oxygen adatoms [two O atoms per (3×4) surface unit cell]. This process can be even faster when the concentration of oxygen increases since, as described above, the barrier for vacancy formation decreases with increasing O coverage. Therefore, we expect the peak temperature for vacancy formation to decrease. These kMC results are in good agreement with experimental observation.

The O-induced vacancy formation discussed above is actually a general phenomenon observed on a number of metal surfaces (see discussion in Ref. [26]). It has been observed also for Ag(111) [54] at much higher temperatures than reported here, in agreement with the fact that higher energy is required to break the more numerous bonds present on Ag(111).

5. Diffusion of free O-Ag-O complex

The diffusion of the detached O-Ag-O complex is anisotropic. The barrier for diffusion of the free complex along [001] is 1.30 eV whereas it is 1.46 eV for the diffusion along [1$\bar{1}$0] (see Fig. 18 for the minimum energy diffusion paths), indicating that the migration of the detached O-Ag-O complex along [001] is slightly preferred. Since the diffusion barriers in both cases are larger than 1 eV, the migration will not be energetically favored at low temperature, unless there is a sophisticated, lower barrier (<1 eV) diffusion path that escapes our calculation. The free complex is therefore robust. The barrier for vacancy migration along [1$\bar{1}$0] is only 0.47 eV, which is smaller than that for the free complex migration along [001]. Moreover, since the free O-Ag-O complex is energetically more favorable than the other O-related structures, these complexes may eventually end up at the location where O and Ag adatoms are involved in added-row formation. The detached free complexes may thus serve as building blocks for added-row structures by forming a 1D chain of O-Ag-O complex along the [001] direction. Indeed, the added rows in the STM images are immobile at 190 K [24], suggesting that these features may be robust at this temperature.

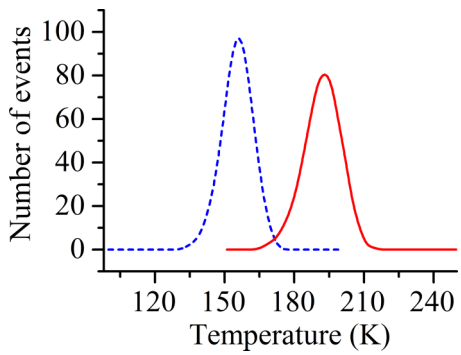

FIG. 17. Kinetic Monte Carlo simulation of Ag vacancy formation (solid) and O_2 dissociation (dashed curve) on Ag(110) at O coverage of 0.16 ML as a function of temperature.

Together with the vacancy formation process discussed in Ref. [26], the above structures, involving a displacement of Ag atoms, may contribute to the surface disorder causing the drop in elastic reflectivity of O/Ag(110) [16] in HREELS experiments.

IV. CONCLUSIONS

Our combined systematic experimental and theoretical analysis has allowed us to unravel the complex structures forming upon O_2 dissociation on Ag(110), which are transiently present under specific reaction conditions. We were particularly interested in identifying a variety of complex O-related features found in our STM measurements: isolated gray dots (G_d), sombreros (S), shallow gray and white (GW) structures oriented along [001] and [1$\bar{1}$0], gray stripes (G), and lozenges (L). The accompanying DFT analysis has identified them, respectively, as isolated O adatoms at FFH sites, O adatoms at LB sites, isolated O adatoms at TFH sites and the embedded O-Ag-O complexes, zigzag rows of O adatoms arranged in TFH sites, and two O adatoms in the valley separated with 2.5 lattice spacing along [1$\bar{1}$0]. At large bias voltages ($V > 0.2$ V), the gray stripes were disrupted giving rise to the formation of sombrero-shaped objects reported, but not assigned, in previous publications on this system [23,24]. Sombreros can be manipulated with electrical pulses at low voltage. The merging of two sombreros gives rise to the GW[1$\bar{1}$0] feature, which corresponds to the O-Ag-O complex embedded in the surface. The DFT-calculated binding energy per O atom ($E_b^{\text{O adatom}}$) suggests that the formation of these O-related features is probable since they differ at the utmost by 200 meV.

The Ag(110) surface requires the presence of oxygen adatoms for the initial phase of local reconstruction which is subsequently followed by Ag atom extraction (formation of a vacancy), and the added-row structure formation. In STM images, the single Ag vacancies are characterized by round-shaped black dots (BDs) with their center at the Ag lattice site, whereas a pair of Ag vacancies are illustrated by an elongated BD with its center at the SB site. Isolated Ag vacancies are mobile, but migrate in an anisotropic manner as suggested by their computed energy barriers of 0.87 eV and 0.47 eV for migration along [001] and [1$\bar{1}$0], respectively. They are thus mobile around 200 K, and can eventually merge together at larger coverage into rather complex, butterfly-shaped features. In short, the presence of O adatoms on the surface is indispensable for vacancy formation (this process can occur at ∼185–190 K as indicated by kinetic Monte Carlo simulation). Strikingly, neighboring O adatoms facilitate Ag atom extraction and help stabilize the mobile Ag atoms in the form of an oxygen-decorated Ag chain along [001] and thus ultimately induce the well-known added-row reconstruction.

ACKNOWLEDGMENTS

We thank Robert Reichelt, Rameez Ud Din, and Angelique Lusuan for helping in different phases of the experiment. We acknowledge the financial support by ICTP through a post-doctoral grant and by Compagnia San Paolo. We acknowledge the STOKES Advanced Research Computing Center at the University of Central Florida, the National Energy Research Scientific Computing Center (NERSC), and the Center for Nanoscale Materials (CNM) of the Argonne National Laboratory for providing the computer resources. T.B.R., S.H., and T.S.R. thank Duy Le for fruitful discussion on simulated STM images and US NSF for partial support under Grant No. CHE-1310327.

[1] W. L. Dai, Q. Liu, Y. Cao, and J. F. Deng, Appl. Catal. A **175**, 83 (1998).
[2] C. T. Campbell and M. T. Paffett, Surf. Sci. **139**, 396 (1984).
[3] J. Serafin, A. Liu, and S. Seyedmonir, J. Mol. Catal. A: Chem. **131**, 157 (1998).
[4] C. Stegelmann, N. C. Schiodt, C. T. Campbell, and P. Stoltze, J. Catal. **221**, 630 (2004).
[5] E. M. Stuve, R. J. Madix, and B. A. Sexton, Surf. Sci. **119**, 279 (1982).
[6] C. F. Mao and M. A. Vannice, J. Catal. **154**, 230 (1995).
[7] Y. Lei *et al.*, Science **328**, 224 (2010).
[8] M. Barteau and R. Madix, J. Am. Chem. Soc. **105**, 344 (1983).
[9] S. Bocklein, S. Gunther, and J. Wintterlin, Angew. Chem., Int. Ed. **52**, 5518 (2013).
[10] S. Günther, S. Böcklein, J. Wintterlin, M. A. Niño, T. O. Menteş, and A. Locatelli, ChemCatChem **5**, 3342 (2013).
[11] T. E. Jones, T. C. Rocha, A. Knop-Gericke, C. Stampfl, R. Schlogl, and S. Piccinin, Phys. Chem. Chem. Phys. **17**, 9288 (2015).
[12] T. E. Jones, R. Wyrwich, S. Böcklein, T. C. R. Rocha, E. A. Carbonio, A. Knop-Gericke, R. Schlögl, S. Günther, J. Wintterlin, and S. Piccinin, J. Phys. Chem. C **120**, 28630 (2016).
[13] M. Rocca, L. Savio, L. Vattuone, U. Burghaus, V. Palomba, N. Novelli, F. Buatier de Mongeot, U. Valbusa, R. Gunnella, G. Comelli, A. Baraldi, S. Lizzit, and G. Paolucci, Phys. Rev. B **61**, 213 (2000).
[14] M. Rocca, L. Vattuone, L. Savio, F. Buatier de Mongeot, U. Valbusa, G. Comelli, S. Lizzit, A. Baraldi, G. Paolucci, J. A. Groeneveld, and E. J. Baerends, Phys. Rev. B **63**, 081404(R) (2001).
[15] L. Savio, C. Giallombardo, L. Vattuone, A. Kokalj, and M. Rocca, Phys. Rev. Lett. **101**, 266103 (2008).
[16] L. Vattuone, M. Rocca, P. Restelli, M. Pupo, C. Boragno, and U. Valbusa, Phys. Rev. B **49**, 5113 (1994).
[17] A. Raukema, D. A. Butler, F. M. A. Box, and A. W. Kleyn, Surf. Sci. **347**, 151 (1996).
[18] L. Vattuone, M. Rocca, C. Boragno, and U. Valbusa, J. Chem. Phys. **101**, 713 (1994).
[19] L. Vattuone, M. Rocca, C. Boragno, and U. Valbusa, J. Chem. Phys. **101**, 726 (1994).
[20] M. Taniguchi, K.-i. Tanaka, T. Hashizume, and T. Sakurai, Surf. Sci. **262**, L123 (1992).
[21] W. W. Pai and J. E. Reutt-Robey, Phys. Rev. B **53**, 15997 (1996).
[22] U. Burghaus and H. Conrad, Surf. Sci. **370**, 17 (1997).
[23] T. Zambelli, J. V. Barth, and J. Wintterlin, J. Phys.: Condens. Matter **14**, 4241 (2002).
[24] T. Zambelli, J. V. Barth, and J. Wintterlin, Phys. Rev. B **58**, 12663 (1998).
[25] M. Smerieri, L. Savio, L. Vattuone, and M. Rocca, J. Phys.: Condens. Matter **22**, 304015 (2010).
[26] J. Pal, T. B. Rawal, M. Smerieri, S. Hong, M. Alatalo, L. Savio, L. Vattuone, T. S. Rahman, and M. Rocca, Phys. Rev. Lett. **118**, 226101 (2017).
[27] L. Savio, A. Gerbi, L. Vattuone, A. Baraldi, G. Comelli, and M. Rocca, J. Phys. Chem. B **110**, 942 (2006).
[28] J. Nowakowski, C. Wäckerlin, J. Girovsky, D. Siewert, T. A. Jung, and N. Ballav, Chem. Commun. **49**, 2347 (2013).
[29] A. Verdini *et al.*, Chem. - Eur. J. **22**, 14672 (2016).
[30] M. Smerieri, R. Reichelt, L. Savio, L. Vattuone, and M. Rocca, Rev. Sci. Inst. **83**, 093703 (2012).
[31] C. T. Campbell and M. T. Paffett, Surf. Sci. **143**, 517 (1984).
[32] H. A. Engelhardt and D. Menzel, Surf. Sci. **57**, 591 (1976).
[33] J. M. Blanco, C. González, P. Jelínek, J. Ortega, F. Flores, R. Pérez, M. Rose, M. Salmeron, J. Méndez, J. Wintterlin, and G. Ertl, Phys. Rev. B **71**, 113402 (2005).
[34] F. Calleja, A. Arnau, J. J. Hinarejos, A. L. Vázquez de Parga, W. A. Hofer, P. M. Echenique, and R. Miranda, Phys. Rev. Lett. **92**, 206101 (2004).
[35] I. Horcas, R. Fernández, J. Gomez-Rodriguez, J. Colchero, J. Gómez-Herrero, and A. Baro, Rev. Sci. Instrum. **78**, 013705 (2007).
[36] G. Kresse and J. Furthmüller, Comput. Mater. Sci. **6**, 15 (1996).
[37] G. Kresse and J. Furthmüller, Phys. Rev. B **54**, 11169 (1996).

[38] J. P. Perdew, K. Burke, and M. Ernzerhof, Phys. Rev. Lett. **77**, 3865 (1996).
[39] P. E. Blochl, Phys. Rev. B. **50**, 17953 (1994).
[40] W.-X. Li, C. Stampfl, and M. Scheffler, Phys. Rev. B **65**, 075407 (2002).
[41] J. Tersoff and D. R. Hamann, Phys. Rev. B **31**, 805 (1985).
[42] J. R. Hahn and W. Ho, Phys. Rev. Lett. **87**, 166102 (2001).
[43] J. R. Hahn and W. Ho, J. Chem. Phys. **122**, 244704 (2005).
[44] J. R. Hahn and W. Ho, J. Chem. Phys. **123**, 214702 (2005).
[45] J. R. Hahn, S. H. Jang, K. W. Kim, and S. B. Son, J. Chem. Phys. **139**, 074707 (2013).
[46] See Supplemental Material at http://link.aps.org/supplemental/10.1103/PhysRevB.98.035405 for a more detailed description of the processes described in Fig. 4.
[47] L. Savio, M. Smerieri, L. Vattuone, A. Gussoni, C. Tassistro, and M. Rocca, Phys. Rev. B **74**, 235412 (2006).
[48] T. B. Rawal, S. Hong, A. Pulkkinen, M. Alatalo, and T. S. Rahman, Phys. Rev. B **92**, 035444 (2015).
[49] N. D. Lang, Phys. Rev. B **34**, 5947 (1986).
[50] N. D. Lang, Phys. Rev. Lett. **58**, 45 (1987).
[51] F. Besenbacher, Rep. Prog. Phys. **59**, 1737 (1996).
[52] P. Stoltze, J. Phys.: Condens. Matter **6**, 9495 (1994).
[53] S. V. Eremeev, A. G. Lipnitskii, A. I. Potekaev, and E. V. Chulkov, Russ. Phys. J. **40**, 276 (1997).
[54] B. V. Andryushechkin, V. M. Shevlyuga, T. V. Pavlova, G. M. Zhidomirov, and K. N. Eltsov, Phys. Rev. Lett. **117**, 056101 (2016).